



A phosphate-rich marine reservoir in the redox stratified Ediacaran ocean

Xiuqing Yang ^{1,2✉}, Jingwen Mao^{1,3}, Fred T. Bowyer⁴, Changzhi Wu¹, Rongxi Li¹, Chao Zhao¹, Guowei Yang¹ & Simon W. Poulton ²

Phosphorus (P) is the key nutrient thought to limit primary productivity on geological timescales, and hence P bioavailability exerted a major influence on Earth's surface oxygenation dynamics through the Precambrian, with ensuing implications for biological evolution. Here, we document highly elevated P contents in non-glacial Ediacaran (635–541 Ma) iron formations from Northwestern China, with P dominantly occurring as carbonate fluorapatite formed during early diagenesis. These analyses, in combination with marine sediment P contents and phosphorite abundance data, point to a state change in oceanic P concentrations during the Ediacaran, which we attribute to enhanced recycling from marine sediments under redox-stratified conditions. Subsequent elevated rates of primary productivity and organic carbon production may have sustained the contemporaneous first appearance of complex deep marine habitats, and would have increased the extent and stability of surface water oxygen concentrations, leading to conditions conducive to the subsequent evolution of more complex animals.

¹MOE Key Laboratory of Western China's Mineral Resources and Geological Engineering, School of Earth Science and Resources, Chang'an University, Xi'an 710054, China. ²School of Earth and Environment, University of Leeds, Leeds LS2 9JT, UK. ³MNR Key Laboratory for Exploration Theory & Technology of Critical Mineral Resources, China University of Geosciences, Beijing 100083, China. ⁴University of Edinburgh, School of GeoSciences, James Hutton Road, Edinburgh EH9 3FE, UK. ✉email: xiuqing2008@126.com

The macronutrient phosphorus is thought to limit primary productivity in the oceans on geological timescales¹, and thus reconstructions of ancient ocean phosphate availability may provide valuable insight into controls on the co-evolution of life and the environment^{2–5}. In modern oceans, the principal source of seawater P derives from continental weathering of phosphate minerals, and this P is subsequently removed to the sediments by biological uptake in the photic zone and sinking of biomass, and via uptake in association with inorganic particles (particularly Fe (oxyhydr)oxides)⁶.

During diagenesis, however, P is commonly remobilized during the microbial degradation of organic matter and during the reductive dissolution of Fe (oxyhydr)oxide minerals^{7,8}. A proportion of this mobilized P may undergo ‘sink switching’ to new authigenic phases, including precipitation as carbonate fluorapatite (CFA)⁸ or vivianite (Fe₃(PO₄)₂)^{9,10}, or via readsorption to Fe (oxyhydr)oxides near the sediment-water interface¹¹. Dependent on the redox state of the sediment porewaters and overlying seawater, however, a proportion of the released P may be recycled back to the water column, where it has the potential to promote a positive productivity feedback^{12,13}. This recycling is particularly prevalent under euxinic (sulfidic) water column conditions, whereas ferruginous (anoxic, Fe-containing) conditions are commonly assumed to promote P drawdown and retention in association with Fe minerals^{4,5,14}, although this behaviour is also dependent on the extent of sulfide generation in shallow sediment porewaters¹⁵.

Reconstructing absolute concentrations of bioavailable water column phosphate in ancient settings is, however, notoriously difficult¹⁶. One approach has relied on P/Fe ratios in iron-rich chemical sediments such as iron formations (IFs), which are considered to reflect contemporaneous dissolved P concentrations in the ocean^{2,3}. However, the precise relationship between P/Fe ratios derived from IFs and dissolved water column phosphate concentrations is complicated by numerous factors, including variable marine silica concentrations through Earth’s history, which influences the uptake of phosphate by Fe (oxyhydr)oxides, but to an extent that is debated^{2,3,17,18}. Prior to the expansion of siliceous phytoplankton in the Phanerozoic, silica concentrations would have been relatively high, although the rock record suggests lower silica concentrations in the Neoproterozoic relative to earlier in the Precambrian¹⁹. Nevertheless, even when taking into account the potential effects of a decrease in silica concentrations in the Neoproterozoic, a major increase in the P

content of IFs indicates a temporal increase in dissolved oceanic phosphate concentrations during the global Cryogenian glaciations³.

Given the discontinuous record of Fe-rich chemical sediments, however, the longer-term significance of a temporal increase in syn-glacial Cryogenian P concentrations is unclear. This limits understanding of the role of P bioavailability during the subsequent Ediacaran, where there is compelling evidence for unstable ocean redox conditions²⁰, including intervals of deep ocean oxygenation accompanying the evolution of the Ediacaran fauna²¹. A more indirect way to assess the P cycle considers the total P content of siliciclastic sedimentary rocks, which has the advantage of a near-continuous record⁴. However, while an initial approach documented a shift to higher marine shale P contents around 800–635 million years ago⁴, an updated shale record suggests little secular change in the median P values of shales deposited through the Neoproterozoic to early Paleozoic, despite a progressive increase in phosphorite deposition²².

The shale record is further complicated by a lack of detailed insight into the intensity of P recycling from marine sediments in the later Neoproterozoic¹⁶, with the heterogeneous nature of ocean redox chemistry potentially having highly variable consequences for the P cycle. Nevertheless, mass balance calculations imply that deep-water phosphate concentrations may have increased by an order of magnitude through the Ediacaran, as a result of rising sulphate concentrations and increased remineralization of organic P by sulphate-reducing bacteria^{22,23}. Previous studies have argued that primary productivity (and thus O₂ production) would have been suppressed by efficient burial of P or limited P recycling in the earlier, oxidant-poor Proterozoic ocean^{24,25}. However, an increase in marine sulphate concentrations and accompanying P recycling during the later Neoproterozoic would be expected to promote enhanced oxygenation^{22,26}, although direct evidence for a persistent rise in later Neoproterozoic marine phosphate concentrations is currently lacking.

Here, we address this limitation by considering newly recognized Ediacaran (ca. 600 Ma) IFs in North Qilian, NW China (Fig. 1). These IFs have only been subjected to very low-grade metamorphism, and are mainly composed of primary hematite and microquartz (jasper)^{27,28}, thus offering a valuable window into contemporaneous Fe and P cycling. To achieve this, we conducted high-resolution petrographic, mineralogical and geochemical studies on the North Qilian IFs, which we subsequently

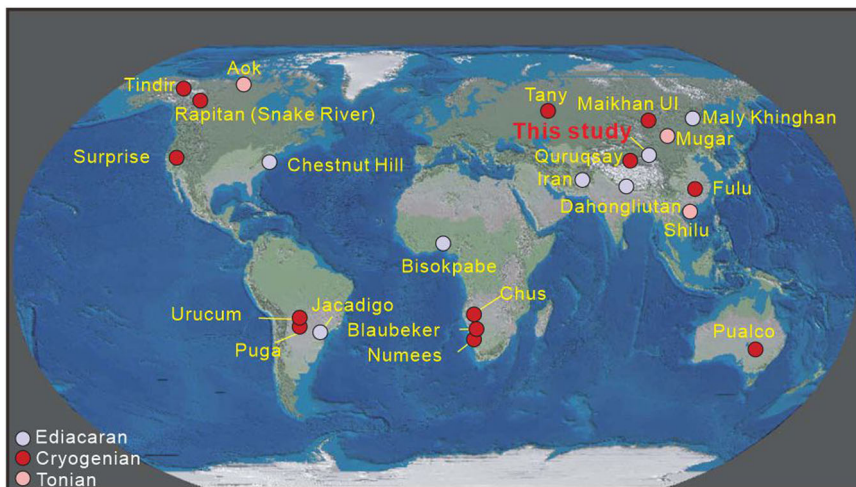


Fig. 1 Present distribution of Neoproterozoic iron formations. Base map from ref. 53, and the location of the Neoproterozoic iron formations from ref. 53,54. Some updated ages of the Neoproterozoic iron formations were listed in Supplementary Table 2.

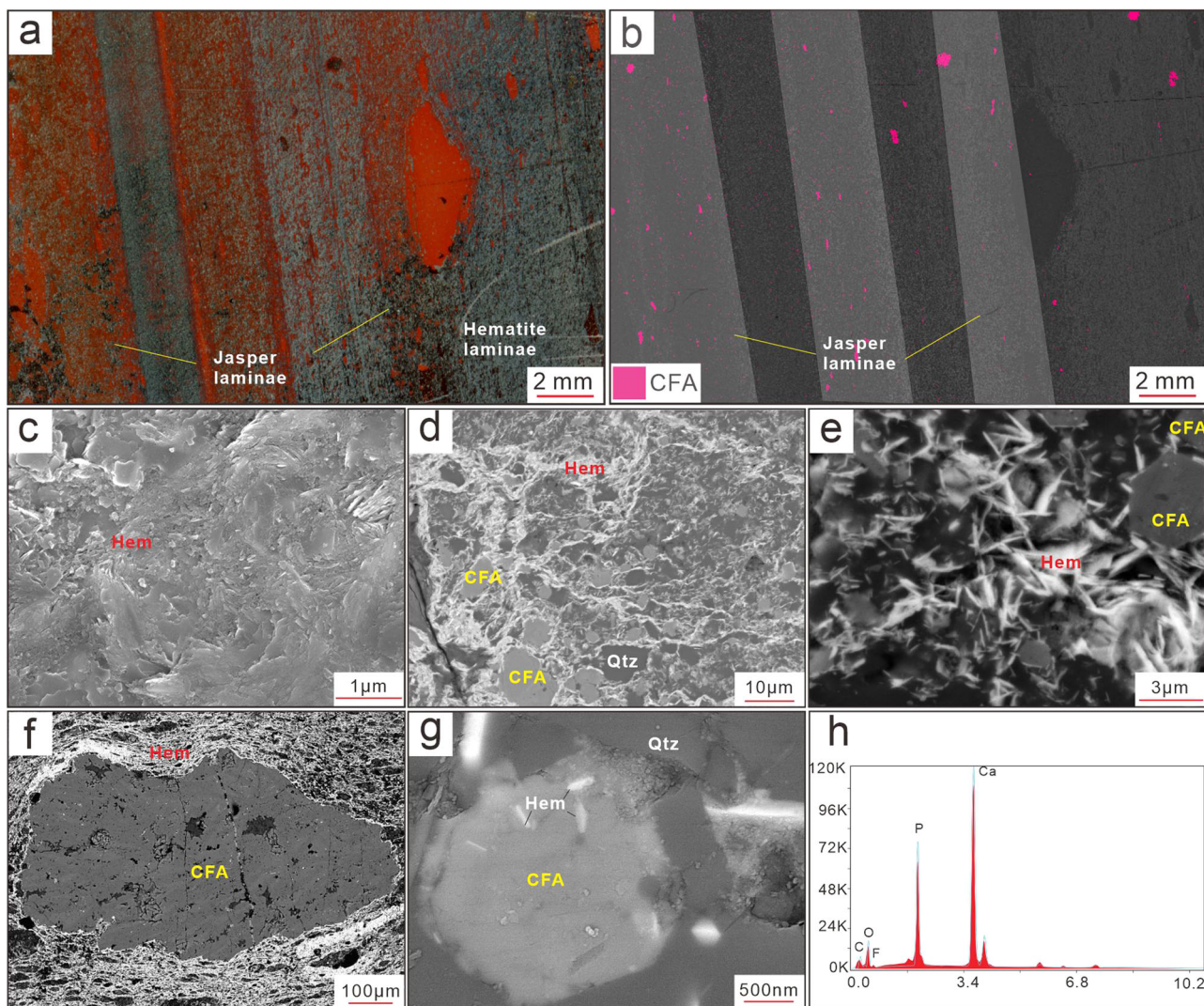


Fig. 2 Photomicrographs of Ediacaran iron formations and carbonate fluorapatite (CFA). **a** Thin section of iron formations with a typical banded structure, where the red laminae are jasper and the gray laminae are hematite (sample JPG-30, banded IF). **b** False-color scanning electron microscope (SEM) mineral map of Fig. 2a, where the red-violet color shows CFA, which is mainly distributed in jasper-rich laminae. **c** SEM photos of fine-grained hematite particles (sample KW-6, IF). **d** Disseminated CFA grains with a subhedral shape (sample KW-33, IF). **e** Euhedral CFA grains (sample JPG-30, banded IF). **f** Rare coarse-grained CFA (sample JPG-28, banded IF). **g** Hematite inclusions in a CFA particle (sample JPG-26, banded IF). **h** EDS spectrum from an apatite particle shown in Fig. 2e, using a gold-plated thin section. Peaks for C, O, F, P and Ca confirm the mineral is CFA. Hem-Hematite, Qtz-Quartz.

place in the context of other global data-sets, allowing a reconstruction of P bioavailability across a critical interval of Earth surface and biological evolution.

Geological background. Several new Ediacaran IFs have recently been identified in the lower Zhulongguan Group of the Qilian Orogenic Belt (Supplementary Figs. 1 and 2), including the Kawa, Jiapigou and Xiaoliugou IFs, which are ~600 Ma in age^{27,28} (see Supplementary Notes 1–3 for further details of the geological setting). These IFs mainly comprise hematite, microquartz (jasper) and minor clay minerals, with rare magnetite, carbonate minerals and apatite (Fig. 2a–g). Banding is generally poorly developed, but when present consists of hematite-rich and jasper-rich laminae, with the width ranging from ~0.5 to 5 mm (Fig. 2a; Supplementary Fig. 3). Kawa, Jiapigou and Xiaoliugou IF samples were collected from open pit mines (Supplementary Fig. 2), with care taken to avoid visible signs of weathering and late-stage hydrothermal alteration.

Results

Petrographic analyses. Where the IFs show a banded/laminated structure (Fig. 2a and b, Supplementary Fig. 4), P-rich grains are clearly present in both hematite-rich and jasper-rich laminae, but are more common in the latter (see Methods for optical techniques). Hematite usually has a dusty (<2 μm) or microplaty (~10 μm) morphology (Fig. 2c), which likely represents the primary Fe mineralogy and its diagenetic product. Minor coarse-grained hematite (long axis >20 μm) is also present, which likely formed during late-stage diagenesis or low-grade metamorphism (see Supplementary Note 4). Element mapping indicates that the P phases are dominantly apatite, with a characteristic high Ca content (Supplementary Fig. 5), which is also consistent with a positive correlation evident between Ca and P concentrations in bulk IF samples (Supplementary Fig. 6a). Energy dispersive spectroscopy (EDS) analyses (Fig. 2h) indicate that the apatite grains are carbonate fluorapatite [CFA, $\text{Ca}_5(\text{PO}_4)_3\text{F}$], which is consistent with previous electron probe micro-analyser (EPMA) studies²⁸. Most CFA grains are less than 5 μm in

Table 1 Summary of phosphorus data for Neoproterozoic iron formations and shales.

Age	Mean	Sd	median	IQR
P/Fe ₍₁₀₀₎ ratios of iron formations				
Ediacaran (635–541 Ma, n = 40)	2.70	2.14	1.89	2.02
Cryogenian (717–635 Ma, n = 144)	1.17	1.24	0.79	1.28
Tonian (1000–717 Ma, n = 14)	0.27	0.25	0.16	0.27
P concentrations of shales				
Ediacaran (635–541 Ma, n = 440)	0.34	1.78	0.03	0.05
Cryogenian (717–635 Ma, n = 245)	0.09	0.10	0.08	0.07
Tonian (1000–717 Ma, n = 628)	0.13	0.54	0.04	0.06

IQR expresses the interquartile range. [P/Fe₍₁₀₀₎ = [mol P]/[mol Fe] × 100]. See Supplementary Tables 2 and 3 for data sources.

diameter (Figs. 2d and e), with rarer grains up to 50 µm (Fig. 2f), and the CFA is usually subhedral-euhedral, although some anhedral intergrowths occur within microplaty hematite (Fig. 2d–g, Supplementary Figs. 4 and 5). Some CFA grains also contain dusty hematite inclusions (Fig. 2g).

Major element and total organic carbon contents. Major element compositions (see Methods for geochemical techniques) are listed in Supplementary Table 1. The samples have high but variable P/Fe₍₁₀₀₎ (P/Fe*100) ratios, ranging from 0.29 to 9.99 (mean = 2.70 ± 2.14). Total organic carbon (TOC) contents are low, ranging from 0.02 to 0.20 wt% (mean = 0.07 ± 0.05 wt%). Published P/Fe₍₁₀₀₎ ratios for IFs, alongside P contents in shales through the Neoproterozoic era (see Supplementary Note 5), are compiled in Supplementary Tables 2 and 3, and these data are summarised for key time periods in Table 1.

Discussion

The behaviour of the P cycle under ferruginous conditions, and particularly during IF deposition, is poorly constrained. Generally low phosphate concentrations in the Proterozoic, where ferruginous water column conditions were commonly widespread^{29–31}, have been suggested to be a consequence of an Fe trap, either through Fe(II)-phosphate precipitation under ferruginous conditions³², or via P uptake during green rust³³ or Fe (oxyhydr) oxide precipitation^{2,18}.

By contrast, through the identification of CFA as the dominant ultimate sink for P in a variety of Archean to Mesoproterozoic IFs and ironstones^{34–37}, alternative hypotheses for the source of P to Fe-rich chemical sediments have been proposed, although little consensus has been reached. Specifically, it has been suggested that P in IFs may have been dominantly derived from the remineralization of biomass, which gave rise to the extremely low organic carbon contents of most IFs, as well as the common presence of reduced secondary minerals such as magnetite and siderite³⁴. However, the low organic content of Precambrian IFs and ironstones has also been used to argue against a significant contribution from P in biomass^{36,37}. Instead, it has been suggested that syndepositional precipitation of Fe(II)-silicate minerals in some Precambrian IFs and ironstones resulted in carbonate fluorapatite (CFA) precipitation being the principal inorganic P sink^{36,37}. This suggestion has been taken to imply that the Archean Ocean contained higher dissolved P concentrations than previously recognized, with a major proportion of the P potentially being supplied by submarine hydrothermal activity³⁷.

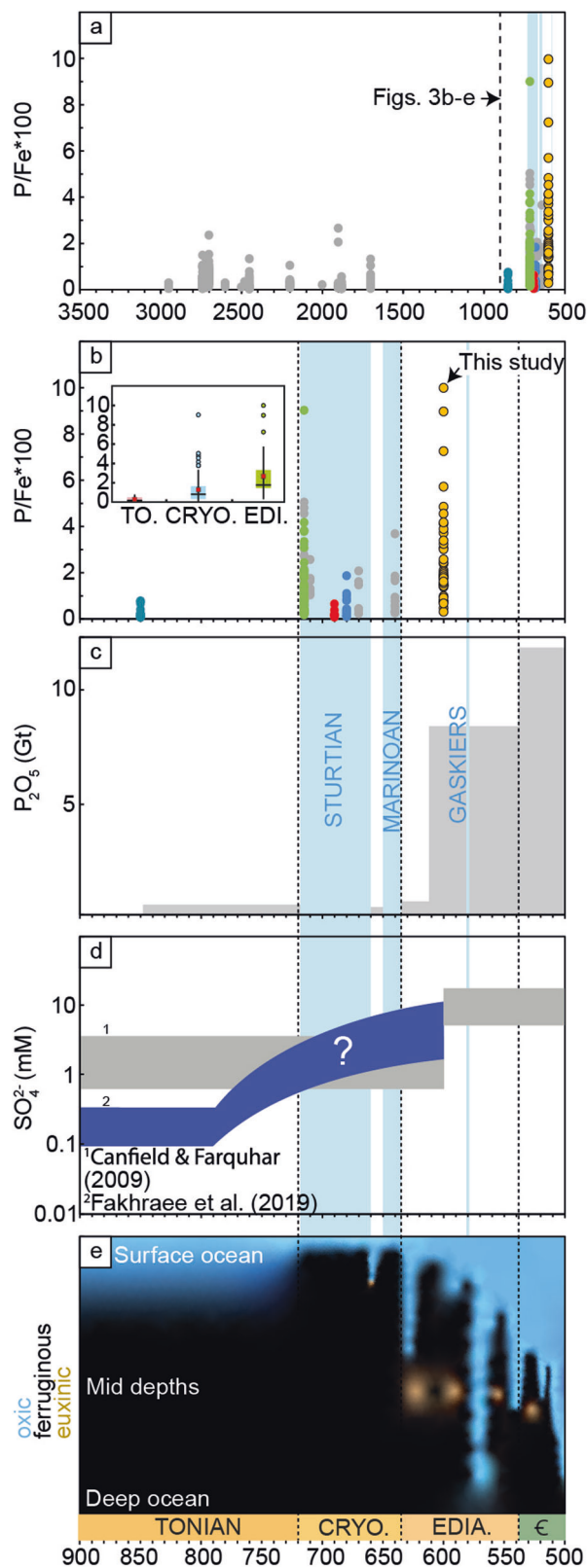
While our SEM-EDS and EPMA analyses demonstrate that CFA was also the dominant terminal sink for P in Ediacaran IFs from North Qilian (Fig. 2h), the precise mechanism for P drawdown from the water column is difficult to unequivocally assign to one particular process (as highlighted by the above

discussion). However, some inferences can be made. First, we note that P concentrations show no correlation with Al in the North Qilian IFs (Supplementary Fig. 6b), suggesting that the P phases were not supplied as detrital particulates, which is consistent with a limited terrestrial mineral contribution to these chemical sediments. We note, however, that this does not preclude a significant proportion of the P being initially sourced from continental chemical weathering³⁶, since continental P that enters solution can be chemically scavenged by the Fe minerals in IFs in a manner unrelated to Al deposition, whereas detrital particulate P would scale with Al.

In addition, while we cannot rule out a contribution of P from organic matter remineralization, which would have led to ‘sink switching’ of P to CFA during early diagenesis⁸, we note that the remobilization of organic carbon via dissimilatory Fe(III) reduction (DIR) would have resulted in the early diagenetic precipitation of Fe(II)-bearing minerals, such as magnetite and siderite³⁸. However, the North Qilian IFs are dominated by hematite with only rare magnetite, suggesting that the oxidation of organic carbon was relatively insignificant (Fig. 2a–e). Thus, it appears unlikely that the exceptionally high P contents of the North Qilian IFs, relative to earlier Precambrian IFs³, resulted solely from P recycling during organic matter remineralization.

The above observations suggest that the primary source of P to the North Qilian IFs was via drawdown in association with Fe minerals. In the North Qilian IFs, the dominance of ‘primary’ hematite implies a hydrous ferric oxide (e.g., ferrihydrite) precursor that likely precipitated in the water column during the oxidation of upwelling ferruginous waters^{27,28}. During this process, co-precipitation and adsorption would have delivered P to the sediment, wherein the early diagenetic transfer of ferrihydrite to more stable hematite (which has a much lower sorptive capacity³⁹) would have released P to the porewaters. In modern hydrothermal sediments, because P adsorbs predictably onto the surfaces of Fe(III) (oxyhydr)oxides, a strong correlation generally exists between Fe and P (Supplementary Fig. 6c)⁴⁰. However, no such relationship is observed in our samples (Supplementary Fig. 6d), which is consistent with observations of P mobilization and incorporation into secondary phases, such as CFA, during the early diagenesis of modern Fe-rich hydrothermal sediments⁴¹. We therefore infer that porewater phosphate concentrations were raised above CFA saturation (which ranges from 20 to >200 µM in modern seawater⁶) by P recycling during the ageing of ferrihydrite to hematite (in addition to a likely minor contribution from organic matter remineralization), thereby promoting CFA deposition (Fig. 2d–f), which is supported by the presence of residual dusty hematite inclusions in CFA grains (Fig. 2g).

We also note that while CFA is present in both hematite-rich and jasper-rich laminae, when banding is present, CFA is particularly common in the latter (Fig. 2, Supplementary Fig. 4). This is also consistent with mobilization of phosphate from Fe minerals during early diagenesis. Indeed, a study of silica-rich



Mesoproterozoic sediments deposited under ferruginous conditions indicated that despite likely supersaturation with respect to vivianite, diagenetically-mobilized phosphate was preferentially precipitated as CFA, which in this specific case was due to removal of aqueous Fe^{2+} from solution during the formation of Fe(II)-silicates such as greenalite and berthierine³⁶. In the case of the North Qilian IFs, the prevalence of solid phase ferric minerals

Fig. 3 Secular variations of P record and ocean chemistry through time.

a $\text{P}/\text{Fe}_{(100)}$ molar ratios for Precambrian iron formations. **b** expanded view of $\text{P}/\text{Fe}_{(100)}$ molar ratios for Neoproterozoic (Tonian, Cryogenian and Ediacaran) iron formations. **c** Size of phosphorite deposits through the Neoproterozoic to Cambrian (900 to 500 Ma)²². **d** Estimated trajectory of oceanic sulphate concentrations through the Neoproterozoic to Cambrian^{55,56}. **e** Schematic representation of the evolution of marine redox state through the Neoproterozoic to Cambrian based on compiled palaeoredox proxy records (adapted after ref. 57).

(i.e., hematite) suggests that Fe^{2+} availability was limited in porewaters, and thus CFA formation was also promoted over vivianite formation.

Notwithstanding the inherent difficulties in using Fe-rich chemical sediments to precisely reconstruct ancient water column P concentrations, it remains likely that general trends through time document first order changes in oceanic P concentrations. Indeed, experiments have shown that a maximum of 10% of the original P in IFs may be remobilized during post-depositional processes⁴², which is far lower than the relative changes observed between the Ediacaran and older IFs (Fig. 3). Four stages have been identified in terms of differing P/Fe ratios, comprising the Quaternary to Cretaceous, Jurassic to Cambrian, Cryogenian, and Paleoproterozoic to Archean³. High $\text{P}/\text{Fe}_{(100)}$ ratios for our Ediacaran IFs (2.70 ± 2.14) are consistent with high ratios for Ediacaran IFs from Iran ($\text{P}/\text{Fe}_{(100)} = 17.7 \pm 12.2$)⁴³, but ratios are considerably higher than for Paleoproterozoic to Archean ($\text{P}/\text{Fe}_{(100)} = 0.37 \pm 0.42$), Tonian ($\text{P}/\text{Fe}_{(100)} = 0.27 \pm 0.25$) and Cryogenian ($\text{P}/\text{Fe}_{(100)} = 1.17 \pm 1.24$) IFs (Fig. 3a, b, Table 1). In addition, the Ediacaran IFs have higher $\text{P}/\text{Fe}_{(100)}$ ratios than Cambrian to Jurassic Fe-rich chemical sediments ($\text{P}/\text{Fe}_{(100)} = 0.38 \pm 0.26$), and are more similar to those deposited during the Cretaceous to Quaternary ($\text{P}/\text{Fe}_{(100)} = 2.55 \pm 1.2$)³.

The order of magnitude increase in Ediacaran $\text{P}/\text{Fe}_{(100)}$ ratios relative to pre-Cryogenian IFs (Fig. 3) strongly suggests highly elevated marine phosphate concentrations at this time, despite the potential competing effects of silica, Ca^{2+} and Mg^{2+} ions on P adsorption to Fe (oxyhydr)oxide minerals^{3,17,18}. We also note that the studied IFs are interlayered with dolostone and sandstone (Supplementary Fig. 2), suggesting they were deposited in a shallow marine setting, thereby eliminating the possibility that they record the higher phosphate concentrations that commonly occur in deeper marine waters^{22,44}. In addition, although the competing effects of variable silica, Mg^{2+} and Ca^{2+} concentrations remain poorly understood for specific time periods, the order of magnitude decrease in $\text{P}/\text{Fe}_{(100)}$ ratios apparent between Ediacaran IFs and Paleozoic-Mesozoic Fe-rich marine sediments (which occurs despite substantially lower silica concentrations in the Phanerozoic ocean¹⁹), implies that the Ediacaran was likely characterized by particularly high dissolved phosphate concentrations.

Consistent with the IF record, the Ediacaran period witnessed one of the largest phosphogenic events in Earth history (Fig. 3c)²². In addition, the mean P content of Ediacaran shales (0.34 ± 1.78 wt%) is significantly higher than shales of the Cryogenian and Tonian (0.09 ± 0.10 wt% and 0.13 ± 0.54 wt%, respectively; Table 1), while carbonates with high P contents also formed during the Ediacaran⁴⁵. The very low $\text{P}/\text{Fe}_{(100)}$ ratios evident in the Tonian IF record (Fig. 3b) is also consistent with a detailed reconstruction of the P cycle in Tonian marine shales⁵, although this contrasts with a diagenetic study of carbonates deposited in the later Tonian⁴⁶. Hence, the precise timing and detailed dynamics of rising phosphate concentrations in the Neoproterozoic remain to be resolved. Nevertheless, multiple observations suggest that high phosphate concentrations in the Neoproterozoic were not limited to the Cryogenian glaciations

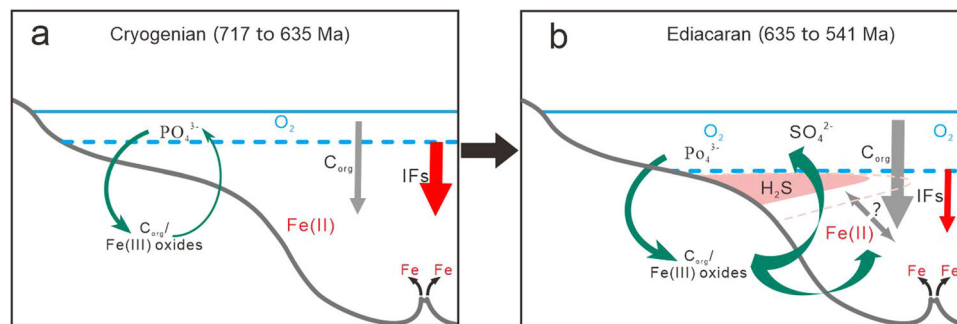


Fig. 4 Cartoon showing the evolution of the oceanic P cycle during the Cryogenian and Ediacaran. **a** During global glaciations of the Cryogenian Period, the ocean was redox stratified and widespread IF deposition occurred. Intense subglacial weathering led to enhanced P/Fe ratios relative to earlier IFs³. **b** During the Ediacaran period, the ocean was also redox stratified. However, the enhanced generation of dissolved sulfide, including the development of water column euxinia in some mid-depth oceanic settings, promoted recycling of phosphate back to the water column. High dissolved Fe^{2+} concentrations in some areas caused local deposition of IFs, which record the high water column phosphate concentrations (via elevated P/Fe ratios).

(c.f. ref. ³). Instead, while Cryogenian seawater witnessed higher P concentrations in association with syn-glacial Sturtian Snowball IF deposition (Figs. 3b and 4a)³, a state change in phosphate concentrations and the global P cycle appears to have occurred during the subsequent Ediacaran period.

A high weathering influx has been proposed as an explanation for the elevated oceanic phosphate concentrations indicated during the Cryogenian glaciations^{3,21}. However, a continued high weathering influx of P through the Ediacaran has not been documented, and instead, a plausible explanation for elevated oceanic phosphorus concentrations is via recycling back to the water column during early diagenesis^{12,13,16}. Our suggestion of phosphate mobilization during hematite formation close to the sediment-water interface indicates the potential for a degree of P recycling. However, the significance of this flux from IFs was likely limited due to their relative scarcity in comparison to normal marine sediments.

On a broader scale, redox-stratified oceans have been widely documented for both the Cryogenian and Ediacaran periods (Fig. 4a and b)^{47,48}. In particular, while ferruginous conditions remained widespread (Fig. 3e), biogeochemical modelling suggests that an increase in oceanic sulphate concentrations during the Ediacaran (Fig. 3d) may have led to enhanced phosphate recycling due to increased remineralization of organic P by sulfate-reducing bacteria²². This would have occurred during diagenesis close to the sediment-water interface, but would have been particularly exacerbated by the enhanced prevalence of mid-depth euxinia (Figs. 3e and 4b), which contrasts with the earlier Neoproterozoic, where a global ferruginous ocean under low sulphate conditions has been proposed as a major limiting constraint on P recycling⁵.

It has also been proposed that recycling of phosphate during microbial sulfate reduction and Fe (oxyhydr)oxide reduction promoted extensive phosphate mineralization in South China⁴⁹. Indeed, redox gradients in marine seafloor sediments are key to phosphogenesis⁵⁰. Modern phosphogenesis occurs almost exclusively in upwelling zones, where deep water supplies the majority of the new nutrient flux to the photic zone⁵¹. In fact, the flux of remineralized P to the surface ocean through upwelling is about 60 times greater than that sourced from rivers⁵¹. Therefore, upwelling of phosphate-rich deeper waters in the Ediacaran likely increased primary productivity in oxygenated surface waters²². This would have ultimately promoted enhanced oxygenation of the upper water column, thus further deepening the redoxcline and creating more expansive, stable, well-oxygenated surface waters. Organic carbon supplied by enhanced primary productivity would also have been a nutrient source for complex multicellular eukaryotes and animals. Indeed, the timing (ca. 600 Ma) of elevated phosphate concentrations recorded by

the IFs analyzed herein coincides (within error) with the minimum age of the Lantian assemblage of South China (602 ± 7 Ma), which constitutes the oldest known Ediacaran macroscopic eukaryotic assemblage⁵².

Our data provide evidence for a persistent step change to higher phosphate concentrations in the Ediacaran ocean. This increase in phosphate was likely driven by redox stratification, particularly through the increased availability of dissolved sulphate and the ensuing enhancement of P recycling from sediments back to the water column. This likely led to enhanced upwelling of phosphate-rich deep waters, ultimately increasing the depth and stability of well-oxygenated waters, while also acting as a nutrient source which likely aided the emergence of complex macroscopic eukaryotes and paved the way for the subsequent evolution of animals.

Methods

Optical microscopy and scanning electron microscopy–energy dispersive X-ray spectroscopy (SEM-EDS), using an FEI Quanta 650 FEG SEM and TESCAN Integrated Mineral Analyzer (TIMA), were employed to identify and characterize phosphate phases in 106 thin sections. For sediment digests, ~50 g was crushed to powder (<74 μ m) for select samples. Powders were dried overnight at 105 °C and then mixed with anhydrous lithium tetraborate–lithium fluoride–ammonium nitrate in a platinum crucible. The mixture was fluxed at 1050 °C, and after cooling, major element concentrations (Si, Ti, Al, Fe, Mn, Mg, Ca, Na, K and P) were determined by x-ray fluorescence using a PW2404 spectrometer, at the ALS Chemex, Guangzhou, China. The analytical error for major elements was 1–3%. Meanwhile, a dry sample aliquot was weighed and ignited for 20 min at 1000 °C in a muffle furnace and then re-weighed to determine the loss on ignition.

Total organic carbon (TOC) measurements were obtained using an infrared absorption method at the Analytical Laboratory of the Beijing Research Institute of Uranium Geology, Beijing, China. 200 mg of sample powder was first treated with HCl in silver capsules to remove carbonate phases. The samples were then combusted in air to release CO_2 , and analyzed using a CS580A analyzer (No. 11022). Accuracy was ensured by replicate analyses of certified reference materials (Soil GBW07407 and Soil GBW07428, with TOC contents of 0.64 ± 0.07 wt% and 0.79 ± 0.07 wt%, respectively), with relative standard deviations of <2%.

Data availability

All data generated during this study are included in the Supplementary Information and are available at figshare database <https://doi.org/10.6084/m9.figshare.24955650>. All data reported in this paper are available in the Supplementary Information.

Received: 9 July 2023; Accepted: 9 January 2024;

Published online: 19 January 2024

References

1. Tyrell, T. The relative influences of nitrogen and phosphorus on oceanic primary production. *Nature* **400**, 525–531 (1999).
2. Bjerrum, C. J. & Canfield, D. E. Ocean productivity before about 1.9 Gyr ago limited by phosphorus adsorption onto iron oxides. *Nature* **417**, 159–162 (2002).
3. Planavsky, N. J. et al. The evolution of the marine phosphate reservoir. *Nature* **467**, 1088–1090 (2010).
4. Reinhard, C. T. et al. Evolution of the global phosphorus cycle. *Nature* **541**, 386–389 (2017).
5. Guilbaud, R., Poulton, S. W., Thompson, J., Husband, K. F. & Lenton, T. M. Phosphorus-limited conditions in the early Neoproterozoic Ocean maintained low levels of atmospheric oxygen. *Nat. Geosci.* **13**, 296–301 (2020).
6. Ruttenger, K. C. The global phosphorus cycle, in Schlesinger, W. H., ed., *Treatise on Geochemistry*, V. 8, Biogeochemistry. Elsevier pp.585–643 (2003).
7. Slomp, C. P., Epping, E. H. G., Helder, W. & Van Raaphorst, W. A key role for iron-bound phosphorus in authigenic apatite formation in North Atlantic continental platform sediments. *J. Mar. Res.* **54**, 1179–1205 (1996).
8. Ruttenger, K. C. & Berner, R. Authigenic apatite formation and burial in sediments from non-upwelling, continental margin environments. *Geochim. Cosmochim. Acta* **57**, 991–1007 (1993).
9. Egger, M., Jilbert, T., Behrends, T., Rivard, C. & Slomp, C. P. Vivianite is a major sink for phosphorus in methanogenic coastal surface sediments. *Geochim. Cosmochim. Acta* **169**, 217–235 (2015).
10. Xiong, Y. et al. Phosphorus cycling in Lake Cadagno, Switzerland: a low sulfate euxinic ocean analogue. *Geochim. Cosmochim. Acta* **251**, 116–135 (2019).
11. Slomp, C. P., Van Der Gaast, S. J. & Van Raaphorst, W. Phosphorus binding by poorly crystalline iron oxides in North Sea sediments. *Mar. Chem.* **52**, 55–73 (1996).
12. Ingall, E. & Jahnke, R. Evidence for enhanced phosphorus regeneration from marine sediments overlain by oxygen-depleted waters. *Geochim. Cosmochim. Acta* **58**, 2571–2575 (1994).
13. Van Cappellen, P. & Ingall, E. D. Benthic phosphorus regeneration, net primary production, and ocean anoxia: a model of the coupled marine biogeochemical cycles of carbon and phosphorus. *Paleoceanography* **9**, 677–692 (1994).
14. Bowyer, F. et al. Regional nutrient decrease drove redox stabilisation and metazoan diversification in the late Ediacaran Nama Group, Namibia. *Sci. Rep.* **10**, 2240 (2020).
15. Alcott, L. J., Mills, B. J. W., Bekker, A. & Poulton, S. W. Earth's great oxidation event facilitated by the rise of sedimentary phosphorus recycling. *Nat. Geosci.* **15**, 210–215 (2022).
16. Poulton, S. W. Biogeochemistry: Early phosphorus redigested. *Nat. Geosci.* **10**, 75–76 (2017).
17. Konhauser, K. O., Lalonde, S. V., Amskold, L. & Holland, H. D. Was there really an Archean phosphate crisis? *Science* **315**, 1234 (2007).
18. Jones, C., Nomosatryo, S., Crowe, S. A., Bjerrum, C. J. & Canfield, D. E. Iron oxides, divalent cations, silica, and the early earth phosphorus crisis. *Geology* **43**, 51–68 (2015).
19. Siever, R. The silica cycle in the Precambrian. *Geochim. Cosmochim. Acta* **56**, 3265–3272 (1992).
20. Bowyer, F., Wood, R. A. & Poulton, S. W. Controls on the evolution of Ediacaran metazoan ecosystems: A redox perspective. *Geobiology* **15**, 516–551 (2017).
21. Canfield, D. E., Poulton, S. W. & Narbonne, G. M. Late-Neoproterozoic Deep-Ocean oxygenation and the rise of animal life. *Science* **315**, 92–95 (2007).
22. Laakso, T. A., Sperling, E. A., Johnston, D. T. & Knoll, A. H. Ediacaran reorganization of the marine phosphorus cycle. *PNAS* **117**, 11961–11967 (2020).
23. Kipp, M. A. & Stüeken, E. E. Biomass recycling and earth's early phosphorus cycle. *Sci. Adv.* **3**, ea04795 (2017).
24. Laakso, T. A. & Schrag, D. P. A small marine biosphere in the Proterozoic. *Geobiology* **17**, 161–171 (2019).
25. Laakso, T. A. & Schrag, D. P. Limitations on limitation. *Glob. Biogeochem. Cy.* **32**, 486–496 (2018).
26. Kipp, M. A. A double-edged sword: The role of sulfate in anoxic marine phosphorus cycling through Earth history. *Geophys. Res. Lett.* **49**, e2022GL099817 (2022).
27. Yang, X. Q. et al. Ediacaran Kawa iron formations in North Qilian Orogenic Belt, Northwestern China: Age, geochemistry, Sm-Nd isotopes and their link with submarine volcanism. *Precambrian Res.* **368**, 106498 (2022).
28. Yang, X. Q. et al. The deposition and significance of an Ediacaran non-glacial iron formation. *Geobiology* **21**, 44–65 (2023).
29. Poulton, S. W. & Canfield, D. E. Ferruginous conditions: a dominant feature of the ocean through Earth's history. *Elements* **7**, 107–112 (2011).
30. Planavsky, N. J. et al. Widespread iron-rich conditions in the mid-Proterozoic ocean. *Nature* **477**, 448–495 (2011).
31. Guilbaud, R., Poulton, S. W., Butterfield, N. J., Zhu, M. & Shields-Zhou, G. A. A global transition to ferruginous conditions in the early Neoproterozoic oceans. *Nat. Geosci.* **8**, 466–470 (2015).
32. Derry, L. A. Causes and consequences of mid-Proterozoic anoxia. *Geophys. Res. Lett.* **42**, 8538–8546 (2015).
33. Zegeye, A. et al. Green rust formation controls nutrient availability in a ferruginous water column. *Geology* **40**, 599–602 (2012).
34. Li, Y., Konhauser, K., Cole, D. & Phelps, T. Mineral ecophysiological data provide growing evidence for microbial activity in banded-iron formations. *Geology* **39**, 707–710 (2011).
35. Pufahl, P. K., Anderson, S. L. & Hiatt, E. E. Dynamic sedimentation of Paleoproterozoic continental margin iron formation, Labrador Trough, Canada: Paleoenvironments and sequence stratigraphy. *Sediment. Geol.* **309**, 48–65 (2014).
36. Johnson, B. R. et al. Phosphorus burial in ferruginous SiO₂-rich Mesoproterozoic sediments. *Geology* **48**, 92–96 (2020).
37. Rasmussen, B., Muhling, J. R., Suvorova, A. & Fischer, W. W. Apatite nanoparticles in 3.46–2.46 Ga iron formations: Evidence for phosphorus-rich hydrothermal plumes on early Earth. *Geology* **49**, 647–651 (2021).
38. Konhauser, K. O. et al. Phytoplankton contributions to the trace-element composition of Precambrian banded iron formations. *Geol. Soc. Am. Bull.* **130**, 941–951 (2018).
39. Liu, J. et al. Adsorption of phosphate and cadmium on iron (oxyhydr)oxides: A comparative study on ferrihydrite, goethite, and hematite. *Geoderma* **383**, 114799 (2021).
40. Wheat, C. G., Feely, R. A. & Mottl, M. J. Phosphate removal by oceanic hydrothermal processes: An update of the phosphorus budget in the oceans. *Geochim. Cosmochim. Acta* **60**, 3593–3608 (1996).
41. Poulton, S. W. & Canfield, D. E. Co-diagenesis of iron and phosphorus in hydrothermal sediments from the southern east Pacific rise: implications for the evaluation of paleoseawater phosphate concentrations. *Geochim. Cosmochim. Acta* **70**, 5883–5898 (2006).
42. Schad, M. et al. Phosphate remobilization from banded iron formations during metamorphic mineral transformations. *Chem. Geol.* **584**, 120489 (2021).
43. Aftabi, A., Atapour, H., Mohseni, S. & Babaki, A. Geochemical discrimination among different types of banded iron formations (BIFs): A comparative review. *Ore Geol. Rev.* **136**, 104244 (2021).
44. Jarvis, I. et al. Phosphorite geochemistry-state-of-the-art and environmental concerns. *Ecol. Geol. Helvetiae* **87**, 643–700 (1994).
45. Shimura, T. et al. In-situ analyses of phosphorus contents of carbonate minerals: Reconstruction of phosphorus contents of sea water from the Ediacaran to early Cambrian. *Gondwana Res.* **25**, 1090–1107 (2014).
46. Roest-Ellis, S. et al. Tonian carbonates record phosphate-rich shallow seas. *Geochem. Geoph. Geosy.* **24**, e2023GC010974 (2023).
47. Li, C. et al. A stratified Redox Model for the Ediacaran. *Ocean. Sci.* **328**, 80–83 (2010).
48. Li, C. et al. Evidence for a redox stratified Cryogenian marine basin, Datangpo Formation, South China. *Earth Planet. Sci. Lett.* **331–332**, 246–256 (2012).
49. Cui, H. et al. Phosphogenesis associated with the Shuram Excursion: Petrographic and geochemical observations from the Ediacaran Doushantuo Formation of South China. *Sediment. Geol.* **341**, 134–146 (2016).
50. Föllmi, K. B. The phosphorus cycle, phosphogenesis and marine phosphate-rich deposits. *Earth-Sci. Rev.* **40**, 55–124 (1996).
51. Schlesinger, W. H. & Bernhardt, E. S. *Biogeochemistry: an analysis of global change*, Academic Press (2013).
52. Yang, C. et al. Implications for Ediacaran biological evolution from the ca. 602 Ma Lantian Biota in China. *Geology* **50**, 562–566 (2022).
53. Hoffman, P. F. et al. Snowball Earth climate dynamics and Cryogenian geology-geobiology. *Sci. Adv.* **3**, e1600983 (2017).
54. Konhauser, K. O. et al. (2017) Iron formations: a global record of Neoproterozoic to Palaeoproterozoic environmental history. *Earth-Sci. Rev.* **172**, 140–177 (2017).
55. Canfield, D. E. & Farquhar, J. Animal evolution, bioturbation, and the sulfate concentration of the oceans. *Proc. Natl. Acad. Sci. USA* **106**, 8123–8127 (2009).
56. Fakhraee, M., Hancisse, O., Canfield, D. E., Crowe, S. A. & Katsev, S. Proterozoic seawater sulfate scarcity and the evolution of ocean-atmosphere chemistry. *Nat. Geosci.* **12**, 375–380 (2019).
57. Wood, R. et al. Integrated records of environmental change and evolution challenge the Cambrian explosion. *Nat. Ecol. Evol.* **3**, 528–538 (2019).

Acknowledgements

We thank two anonymous reviewers for their constructive comments. This work was supported by the National Natural Science Foundation of China (Nos. 41972075 and 41702063) and the Fundamental Research Funds for the Central Universities, CHD (No. 300102272203). There are no sampling permissions required. We are grateful to Miao Yu and Wenlei Song for their assistance with the SEM-EDS analyses. Finally, we thank the editor and two anonymous reviewers for their valuable comments.

Author contributions

X.Q.Y. and J.W.M. conducted the design and analyses. X.Q.Y. and G.W.Y. performed the fieldwork. C.Z.W., R.X.L. and C.Z. compiled the data. All authors contributed to the interpretation of the results. X.Q.Y., J.W.M., F.B. and S.W.P. wrote the manuscript, with contributions from all authors.

Competing interests

The authors declare no competing interests.

Additional information

Supplementary information The online version contains supplementary material available at <https://doi.org/10.1038/s43247-024-01211-2>.

Correspondence and requests for materials should be addressed to Xiuqing Yang.

Peer review information *Communications Earth & Environment* hanks the anonymous reviewers for their contribution to the peer review of this work. Primary Handling Editors: Mojtaba Fakhraee, Joe Aslin and Aliénor Lavergne. A peer review file is available.

Reprints and permission information is available at <http://www.nature.com/reprints>

Publisher's note Springer Nature remains neutral with regard to jurisdictional claims in published maps and institutional affiliations.



Open Access This article is licensed under a Creative Commons Attribution 4.0 International License, which permits use, sharing, adaptation, distribution and reproduction in any medium or format, as long as you give appropriate credit to the original author(s) and the source, provide a link to the Creative Commons licence, and indicate if changes were made. The images or other third party material in this article are included in the article's Creative Commons licence, unless indicated otherwise in a credit line to the material. If material is not included in the article's Creative Commons licence and your intended use is not permitted by statutory regulation or exceeds the permitted use, you will need to obtain permission directly from the copyright holder. To view a copy of this licence, visit <http://creativecommons.org/licenses/by/4.0/>.

© The Author(s) 2024